

Study of a Flow-Induced-Vibration Energy Harvester: A Case of Two-degree of Freedom Galloping Based Scheme

Ankit Gautam ^a, Mahesh Chandra Luintel ^b

^{a, b} Department of Mechanical and Aerospace Engineering, Pulchowk Campus, IOE, Tribhuvan University, Nepal

Corresponding Email: ^a ankitgautam@pcampus.edu.np, ^b mcluintel@ioe.edu.np

Abstract

The energy harvester based on galloping is an appropriate means to convert flow-induced vibration to electric energy at the small wind speed. The study aims to expand the energy extraction of galloping based piezoelectric energy harvester (GPEH) by using two degrees of freedom (DOF) based GPEH over the normal one degree of freedom based GPEH. The optimum secondary beam was attached to the primary beam of one degree-of-freedom GPEH to design the two-degree-of-freedom GPEH and the results are compared in terms of power peaks and efficiency. The performance analysis of the two-DOF GPEH system has been done with respect to tip mass and the position of the secondary beam. The designed models are numerically analyzed in ANSYS using a Realizable k- ϵ turbulent model along with the two-way coupled fluid-structure interaction simulations. The result shows that the maximum power peaks increased by 15.88% and the efficiency improved by 0.972%. The results from the performance test of the two DOF GPEH suggest that the optimum position for the secondary beam is close to unfixed end of the primary beam at 0.75D. Moreover, the tip mass has a rare change in power peaks at low tip mass while higher tip mass causes to decrease in the harvested power.

Keywords

Galloping Energy Harvester, Flow-induced vibration, Two-DOF GPEH, Fluid-Structure Interaction

1. Introduction

The flow-induced vibration is the general phenomenon of applied concentration in numerous engineering areas (transmission wires, bridges, lightning poles) and have the potential to harvest electrical energy efficiently from low-speed wind [1]. The mechanism of harvesting wind energy needs to translate energy in airflow into vibration energy on the structure or any object using different flow-induced vibration phenomenon. Practically the flow induced vibration types used for the energy extraction are galloping, wake galloping, flutter and vortex-induced vibration [2]. The structural vibration energy is achieved using an oscillating bluff body directed to wind flow. Then this vibration energy on structure is transformed to electric energy through several means such as electromagnetic, electrostatic and piezoelectric effect[3]. Energy extraction through piezoelectric device is the extensively used technique due to its comfort in implementation, comparatively large yield in voltage, and developed construction[4].

The piezoelectric energy harvester based on galloping is extensively researched because of having large oscillating amplitude and a widespread choice of working air speed[5].

An ordinary GPEH can be created as an oscillating harvester by connecting a bluff object to the unfixed end of the flexible beam presented in the Figure 1, on the flexible structure piezoelectric patch is attached to absorb the vibration. The fluid-solid interplay phenomenon (at the interface of air and structure) causes to generate a lift force on a bluff body. The direction of an aerodynamic lifting force is orthogonal to the direction of air flow and acts similar to undesirable damping expression, and this damping is the crucial to generate self-exciting vibration of the structure. The energy extraction scheme, GPEH can be modelled as a one or a two degree of freedom (DOF) scheme as exposed in Figure 2, in past, the one-DOF scheme was widely used while the two-DOF system is the recent topic of research in GPEH[6, 2]. The Figure 2 displays both the model; one and two degree of freedom scheme GPEH. The

single degree of freedom scheme consists of a flexibly joined bluff object along with the piezoelectric sensing device. It experiences galloping in a crossway direction when exposed to the airflow. In the two-DOF GPEH, a secondary one-DOF oscillator is added on the top of the one-DOF model. [7]

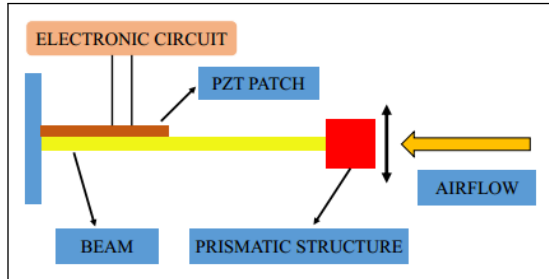


Figure 1: Schematic of GPEH [8]

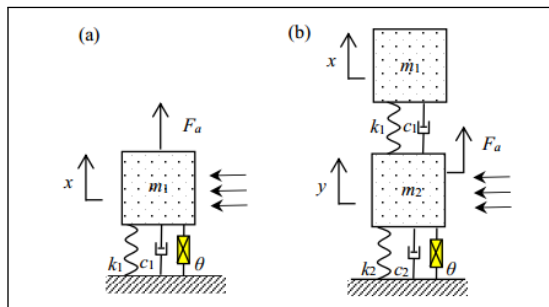


Figure 2: (a) 1-DoF and (b) 2-DoF System [6]

2. Literature Review

The mechanism of galloping was studied and explained in 1943 by Den Hartog for the first time [9]. In his study, the aerodynamics force was described using the quasi-steady hypothesis. [10] did a theoretical analysis on the potential use of transverse galloping for the purpose of obtaining useful energy. One DOF model was used for the investigation and the effect of cross-sectional setup along with the physical behavior on the electricity production were studied. [11] inspected wind EH from galloping with cross-section of D-shape by means of a beam with piezoelectric sensing device fixed to a tip body. They stated the rise in air speed, increases the power production significantly. Also, they determined that a critical speed of 5.6 mph is needed for harvesting energy and found highest produced power to be 1.14 mW at a air speed of 10.5 mph. [12] studied the influence of a Reynolds number on the galloping of square cylinder to produce energy. They showed that a Reynolds number and resistance had significant impact on the amount of power production.

Using the harmonic balancing technique, [6] investigated the dynamics and energy harvesting performance of a two DOF configuration as well as their possible benefit comparing to the ordinary one-DOF GPEH. It is shown that a second arrangement of two DOF can simply minimize the critical speed of wind and greatly enhance the power production of wind energy harvesting, which is very capable for boosting the efficiency of extracting wind energy. While they stated that the first arrangement of two DOF increases the critical speed and decrease power at lower speed. [13] did the numerical study on the extraction of energy through aeroelastic mechanism based on one DOF galloping mechanism. [2] tested the energy extracted from a two-degree of freedom galloping mechanism in an experimental investigation. They demonstrated that adding an extra beam reduced the critical wind speed to 1.961 m/s from 2.372 m/s, and they recorded 11.11% increase in a power production using a most acceptable two-degree of freedom GPEH over a standard one-degree of freedom GPEH.

In previous studies, [4, 5, 7, 10, 11, 12, 13] of energy harvesters based on galloping are of one DOF system. The two DOF GPEH done in [6] using harmonic balance method is an analytical study and the study done in [2] is only an experimental study done only on one configuration. The study done by [2] is the first arrangement of two DOF done by [6], in which Lan et.al. showed an increase in critical speed and decrease in power output, while Hu et.al. showed a decrease in the critical speed and increase in power. There is a need for research to identify the contradiction between these two studies. Therefore, a better approximation of the parameters of the system can be carried out for a two DOF galloping-based energy harvester using transient two-way FSI analysis: simultaneous CFD analysis and structural analysis. The comparative analysis of one DOF and two DOF is required with respect to power production and efficiency. Moreover, the parametric study should be done in terms of wind speed, tip mass, and orientation of the secondary beam focusing to identify an exact performance of a two DOF GPEH.

3. Mathematical Modelling of GPEH

3.1 Physical Mechanism

One-DOF GPEH system in Figure 2(a) shows a spring supported model exposed to the steady flow of

velocity U and density ρ . c_1 indicates damping, m_1 is mass, and k_1 indicate stiffness of a one DOF GPEH, θ is a coefficient for electromechanical coupling, C_p represents the equivalent capacitance of a piezoelectric sensor, x is the displacement covered from the bottom and F_a is an aerodynamic lifting force reacting on the bluff object vertically. A governing equation relied upon the approximation of electromechanical coupling to be linear with elastic characteristics is given in Equation 1, where V indicates a voltage generated by a piezoelectric sensing device and R , load resistance of the device. The aerodynamic force F_a given by [10] are also shown in Equation 1, in this equation, L is the length along the transverse of air flowing direction and D is width of the tip object, a terms with S , s_1 and s_3 are the ideal coefficient of a lifting load, suffice 1 indicates linear coefficient and suffice 3 indicate cubic coefficient, and they are reliant on a physical geometry of the bluff bodies.

$$\begin{cases} m_1\ddot{x} + c_1\dot{x} + k_1x - \theta V = F_a \\ C_p\dot{V} + \frac{V}{R} + \theta x = 0 \\ F_a = \frac{1}{2}\rho U^2 LD [s_1 \frac{\dot{x}}{U} - s_3 (\frac{\dot{x}}{U})^3] \end{cases} \quad (1)$$

After derivation, the critical velocity for the onset of the galloping instability for one-DOF GPEH is shown in Equation 2

$$\begin{cases} U_{crit} = \frac{2(c_1 + c_e)}{\rho LDS_1} \\ c_e = \frac{\theta^2 R}{(C_p R \omega)^2 + 1} \end{cases} \quad (2)$$

Similarly, Equation 3 contains the equations that governs the kinetics of a two DOF galloping EH system as depicted in Figure 2(b). Where, c_2 , m_2 , k_2 and y indicates the primary structure's damping, mass, stiffness and displacement respectively[6].

$$\begin{cases} m_1\ddot{x} + c_1(\dot{x} - \dot{y}) + k_1(x - y) = 0 \\ m_2\ddot{y} + c_2\dot{y} + k_2y - \theta V = \frac{1}{2}\rho U^2 LD [s_1 \frac{\dot{x}}{U} - s_3 (\frac{\dot{x}}{U})^3] \\ + c_1(\dot{x} - \dot{y}) + k_1(x - y) \\ C_p\dot{V} + \frac{V}{R} + \theta y = 0 \end{cases} \quad (3)$$

After derivation, the critical wind speed for the onset of the galloping instability for two-DOF GPEH scheme is given in Equation 4.

$$U_{crit} = \left[2(c_2 + c_e) + \frac{2(m_1\omega^2)^2}{(k_1 - m_1\omega^2)^2 + (c_1\omega)^2} c_1 \right] / (\rho LDS_1) \quad (4)$$

3.2 Governing Equations

The codes of CFD are built on numerical technique and process for dealing with problems of fluid-flow. A finite volume method was used for the discretization of algebraic expressions. The Equation 5 below describes the continuity and Navier Stokes equations.

$$\begin{cases} \frac{\partial \rho}{\partial t} + \Delta(\rho \vec{V}) = 0 \\ \frac{\partial}{\partial t}(\rho \vec{V}) + \Delta(\rho \vec{V} \vec{V}) = -\Delta P + \Delta(\vec{\tau}) + \rho \vec{g} + \vec{F} \\ \vec{\tau} = \mu [(\Delta \vec{V} + \Delta \vec{V}^T) - \frac{2}{3} \Delta \vec{V} I] \end{cases} \quad (5)$$

In Equation 5, $\vec{\tau}$ is the stress tensor vector, a static pressure is indicated by P , and $\rho \vec{g}$, \vec{F} are the forces term, first is due to gravity and second is due to external applied force. For turbulent modeling Realizable $k-\varepsilon$ scheme was implemented for its good behavior in freestream flows. The realizable $k-\varepsilon$ model is two equation model and has two extra transport equations shown in Equation 6 to solve turbulent kinetic energy term k and a dissipation rate term ε [14].

$$\begin{cases} \frac{\partial}{\partial t}(\rho k) + \frac{\partial}{\partial x_j}(\rho k u_j) = \frac{\partial}{\partial x_j}[(\mu + \frac{\mu_t}{\sigma_k}) \frac{\partial k}{\partial x_j}] + E \\ \frac{\partial}{\partial t}(\rho \varepsilon) + \frac{\partial}{\partial x_j}(\rho \varepsilon u_j) = \frac{\partial}{\partial x_j}[(\mu + \frac{\mu_t}{\sigma_\varepsilon}) \frac{\partial \varepsilon}{\partial x_j}] + Q \\ E = G_k + G_b - \rho \varepsilon - Y_M + S_k \\ Q = C_{1\varepsilon} \frac{\varepsilon}{k} C_3 \varepsilon G_b + \rho C_{1\varepsilon} S_\varepsilon - \frac{C_2 \rho \varepsilon^2}{k + \sqrt{\nu \varepsilon}} + S_\varepsilon \end{cases} \quad (6)$$

3.3 Two-way Coupling

In the designed system, wind dynamics impacts the bluff body and a beam as well as the wind dynamics is affected by the displacement of the bluff body and the deformation of beam. A calculation of two-ways couplings comprises the process of transferring the displacement of the structural solver to the fluid solver as presented in Figure 3[15].

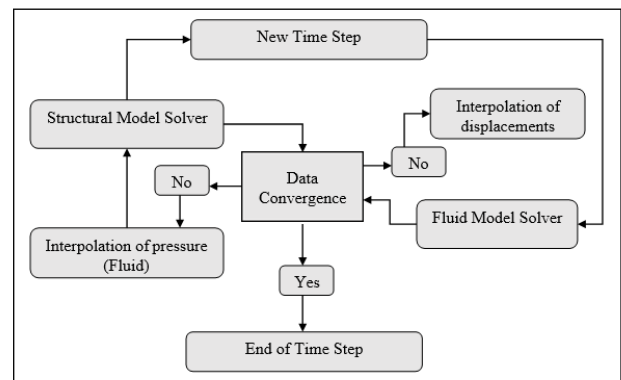


Figure 3: Two-way Coupling methodology

3.4 Piezoelectricity

The stress and deformation developed on the piezoelectric materials is converted to the electric energy due to its electromechanical phenomenon. A governing piezoelectric constitutive equation for direct and converse piezoelectric effects are given in Equation 7 [8].

$$\begin{bmatrix} \delta \\ D \end{bmatrix} = \begin{bmatrix} S^E & s^t \\ d & \epsilon^T \end{bmatrix} \begin{bmatrix} \sigma \\ E \end{bmatrix} \tag{7}$$

4. Geometry

The geometry of the physical setup is shown in Figure 4. The fluid domain is a rectangular prism having a cross-section area of 600 mm * 600 mm and a length of 1200 mm. In this study, at first, the one DOF GPEH model is designed followed by two DOF galloping EH by adding second beam to perform the comparative study. For the one-degree of freedom GPEH model, beam’s first end is fixed and another end is free with a bluff object. The material composition of beam is 140mm long aluminum, a width of 20mm and 0.5 mm thick. The fundamental natural frequency should not be very high according to the galloping EH design criteria and aluminium is suitable for this. The bluff body is made of polyurethane with a cuboid shape having a dimension of 140*32*32 mm³ having tip mass of 30 gm.

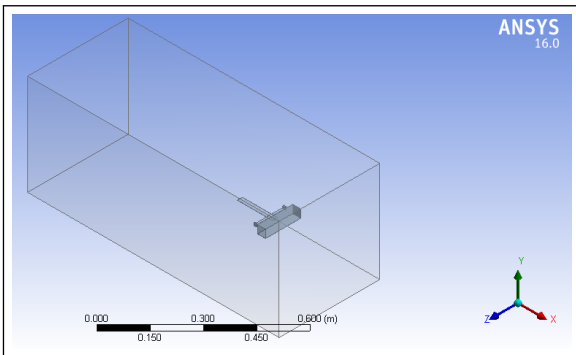


Figure 4: Geometry for two-DoF GPEH

In two DOF Galloping EH, the second beam is symmetrically mounted to the primary beam of the one DOF GPEH system. The inelastic deformation must be avoided during vibration in the second beam as per a second beam’s design criteria. To avoid the plastic deformation in the secondary beam, it is made of steel having higher yield strength. The length of the secondary beam is 120mm having a width and

thickness of 8mm and 0.1 mm respectively. As the end masses, the polyurethane cuboids having a total mass of 12 gm are fastened at extreme ends of the second beam.

5. Numerical Simulations

In this study, the purpose of the numerical simulation is to calculate the displacement in the structural setup at a given wind velocity throughout the flow time. The simulation work of this research was carried out in two parts, the first part deals with the CFD model and the other with the structural model. For this, the fluid domain and structural setup were imported from the 3D CAD software, CATIA. The meshing of the models was done using ANSYS Meshing for both fluent analysis and structural mesh. The fluid domain was divided into two parts for assigning multiple methods and parameters of meshing like orthogonal quality and aspect ratio, were continuously monitored to achieve a mesh independent solution. The fully generated mesh of fluid domain and structural mesh is shown in Figure 6 and Figure 7. Numerical studies were done iteratively with the refinement of the mesh. The solution must tends to meet at a point and the needed result specifications must not depending on divided parts of the fluid field for any numerical results to have less amount of error[16]. Figure 5 shows a grid independence graph. As per the grid convergence analysis the number of nodes for all the analysis was set to be around 300,000 since further refinement in the mesh would have only increased the computational time.

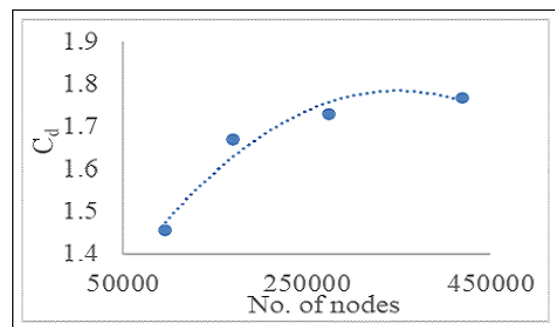


Figure 5: Mesh Independence Test

The ANSYS CFD code FLUENT was used to discretize the governing equation with the Finite Volume Method for the CFD analysis. For turbulent modelling, Realizable k-ε was used with first-order upwind in kinetic energy and dissipation rate in

first-order upwind. The fluid model is comprised of air having a value of 1.225 kg/m^3 and 1.789×10^{-5} as a mass density and dynamic viscosity respectively. The structural member is comprised of Aluminium having a value of 71 GPa as Young's Modulus of elasticity, mass density of 2770 kg/m^3 , and Poisson's ratio is 0.33. To find the solution of mathematically separated equations, implicit technique and steady pressure based segregated solver with double precision has been employed. For the steady terms, the second-order method was taken. A discretized equations were solved by using a coupled scheme. A mathematical separation of a momentum equation along with other mathematical expression was settled through upwinding scheme of second order. This technique helps to exhibit an appropriate process of the motion fluid. A transient simulation has been done to find a performance of galloping EH with variable tip mass, velocity and position of secondary beam. The inlet is the velocity inlet, the outlet is the pressure outlet that is exposed to the atmospheric pressure and the wall of the fluid domain are taken fixed without any slip. A outside surface of a bluff bodies is considered as a fluid-solid wall with dynamic mesh settings that have to be added to these surfaces in order to get a mesh deformation in which the important step is to assign a dynamic mesh zone among the boundaries of a fluid model.

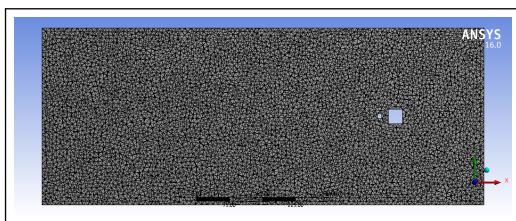


Figure 6: Meshing for Fluid Solver

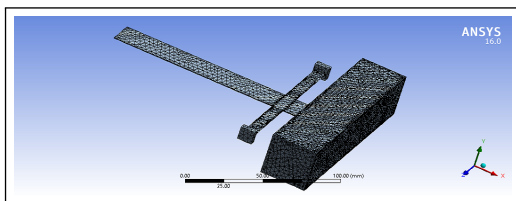


Figure 7: Meshing for Structural Solver

6. Results and Discussion

6.1 Comparative Study

The one DOF system and two DOF system were compared with respect to the amount of power

harvested and the system's efficiency. To calculate the power produced by the system, the y-displacement obtained from the simulation was used to calculate the voltage generated which in turn was used to calculate power produced by the GPEH. Piezoelectric sheets having coupling term $\theta = 1.55 \text{ mN/V}$ and the equivalent capacitance of $C_p = 120 \text{ nF}$ are used. To calculate the efficiency of the system the input power was calculated using air flux impacted under the active area of the system.

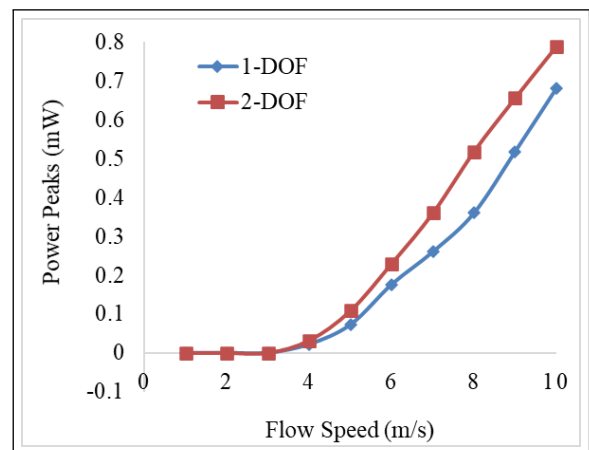


Figure 8: Power Peaks Vs Flow Speed Plot

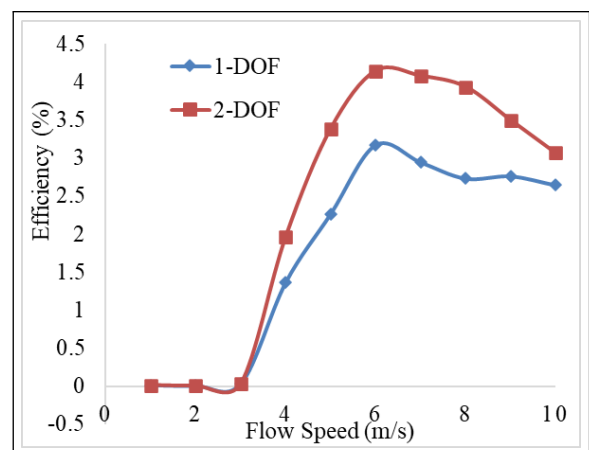


Figure 9: Efficiency Vs Flow Speed Plot

To study the effect of using the two DOF GPEH in comparison with the one DOF GPEH system the power peaks vs flow velocity and efficiency vs flow velocity was plotted in Figure 8 and Figure 9 respectively. It is noted that the critical air speed for the two DOF systems is lesser compared to one DOF counterpart. Power produced by feeding 10 m/s flow speed is 0.788 mW for the two DOF system while the power produced by the one DOF system is 0.680 mW, showing the 15.88% increment. The efficiency of GPEH is very

low at low wind speed, high in the region slightly above the critical flow speed, and decrease at larger flow speed. The highest efficiency achieved for the 2-DOF system is 4.146% while for the one DOF system the highest efficiency achieved was 3.175%.

6.2 CFD Results of two DOF GPEH

The CFD simulations have been done to know the state of the two DOF system at different time steps. The inlet velocity of 10 m/s was applied at the inlet to investigate the effect of transient states. Figure 10 and Figure 11 shows the instantaneous pressure field and velocity field respectively at the time step 0.1, 0.3 and 3s. The flow’s stagnation point is situated on the fore-end of a bluff object, leading to a high-pressure difference in the horizontal direction. Also, at the same time, flow separation starts from the upper side and the lower side of the structure. It has global minimum pressure of -321.7 Pa and a maximum pressure of 112 Pa. The pressure starts to decrease in a steady way towards the downstream. The flow separation begins from the upper side and lower side of the structure and starts to oscillate in the wake region after 0.3 secs. In the region, just after the flow separation, a maximum velocity of 21.07 m/s is noted.

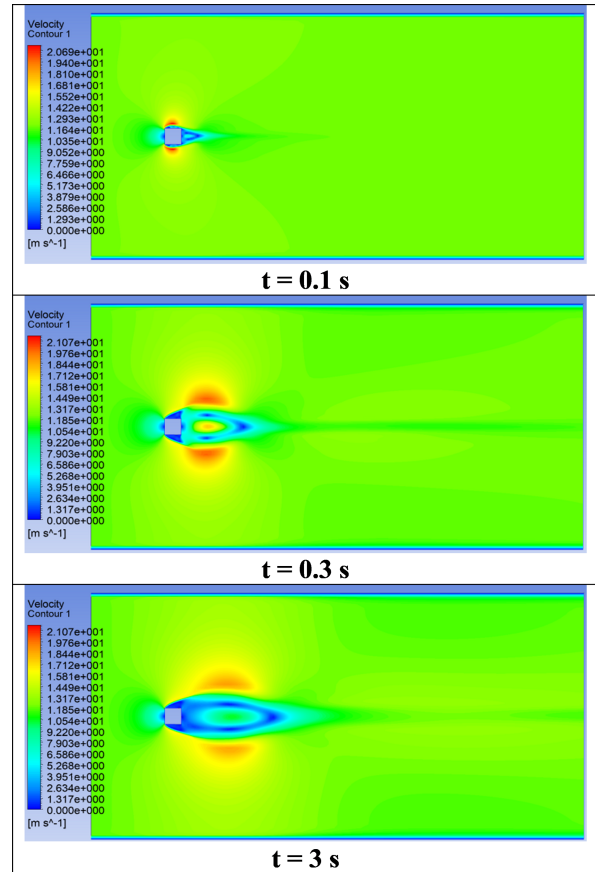


Figure 11: Velocity at different timestep

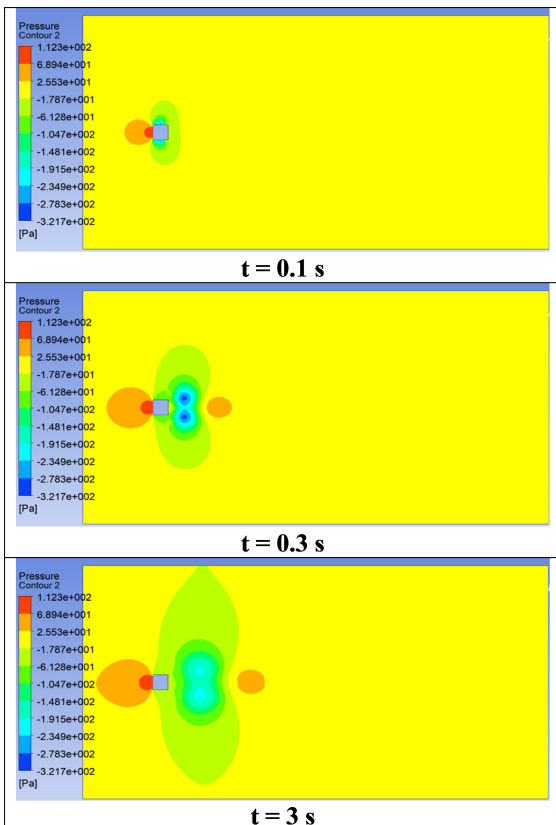


Figure 10: Pressure contour at different timestep

6.3 Performance Analysis of two-DOF GPEH

The performance of the two DOF GPEH system was evaluated with respect to secondary beam’s position and the primary beam’s tip mass, and power peaks is used as performance indicator.

6.3.1 Effect of position of secondary beam

Figure 12 shows the power peaks of two-degree of freedom galloping EH for the several positions of the secondary beam measured from a primary beam’s unfixed end. Effect of secondary beam’s position was investigated from 0.25D to 2.5D, where D is kept at 32 mm in this study. When the separation between the primary beam’s unfixed end and the attachment of the secondary beam is extended, output power increases slightly. However, the large distance causes a significant decrease in power production. This decrease in the power production is due to the effect of high aerodynamic load on object attached on secondary beam. An optimal position of secondary beam can be obtained for a two DOF GPEH system, it should be in proximity of primary beam’s unfixed end. In this investigation, output power was high at 0.75D.

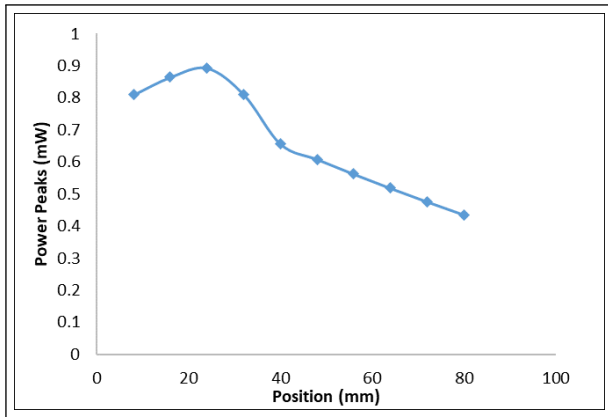


Figure 12: Power peaks at different position of secondary beam for 2-DOF GPEH

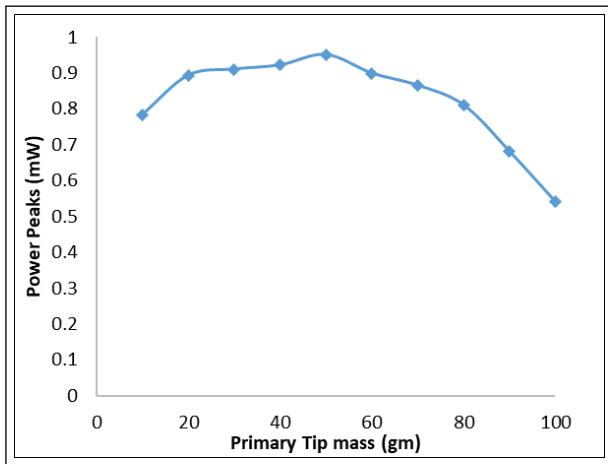


Figure 13: Power peaks at different tip mass for 2-DOF GPEH

6.3.2 Effect of Tip-Mass

Mass at beams end is always pivotal for the dynamics of galloping energy harvester mechanism. The effect of primary beam’s tip-mass on the energy harvested was evaluated and shown in Figure 13. The change in tip-mass was made by making changes in density of a bluff object and air flow velocity for this purpose was kept at 10 m/s. It can be noted that the increase in mass at beam’s end affect power extraction for low tip-mass conditions. The curve is flat for the change in tip mass indicating that tip mass rarely affects the power output for moderate tip mass conditions. When the tip mass becomes large the power output starts to decrease as the high inertia causes difficulty in the oscillation. An optimal tip mass can be obtained for the two DOF GPEH system which can obtain maximum power with specific air speed. The highest power peak obtained was 0.951 mW at a tip mass of 50 gm.

7. Result Validation

The previous studies on two DOF are experimental study by [2] and analytical study by [6]. The exploration of the contradiction mentioned in section 2 from this study suggest that the critical speed decreases and power increases for two DOF system as of [2]. Therefore, the result obtained from the numerical analysis is validated by comparing with the experimental results obtained in [2] for the two DOF GPEH. The modelling of the two DOF GPEH system was done similar to the modelling done in that study for validation. The voltage generated vs flow speed was plotted to show the comparative results and presented in Figure 14. The patterns of voltage generated from this study are similar to that study, and the critical air speed was achieved from both studies were in span of 2 m/s and 4 m/s. However, voltage generated from this study are higher than those obtained in the experimental study. This is because of the error that occurred due to operational challenges in the experimental study. The aerodynamic load on the beam surface is pivotal in adding errors between the numerical study and experimental study. The maximum voltage generated for two DOF GPEH in this study and the experimental study are 35.52 V and 26 V respectively.

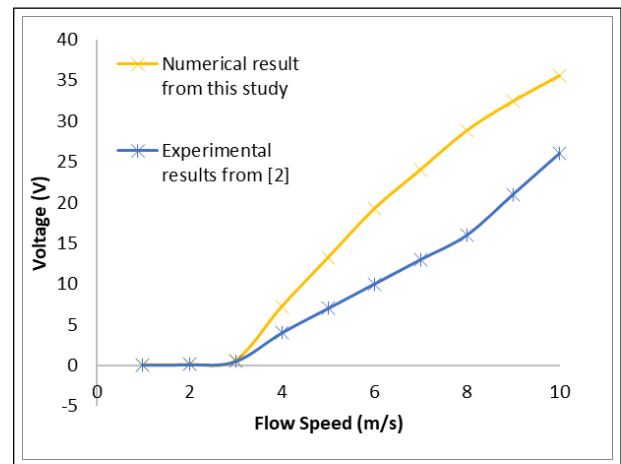


Figure 14: Voltage Vs Flow Speed for validation

8. Conclusion

The study numerically investigated the way to increase the performance of GPEH by using a two DOF system, which is capable of extracting the utmost energy through flow-induced vibration. Performance analysis of two DOF GPEH was done with two-way FSI simulation and the numerical result

was validated through the experimental data obtained from [2]. The 15.88 % increase in power production and improvement of 0.972 % efficiency was achieved by using two DOF galloping EH over ordinary one DOF galloping EH. Two DOF GPEH system has critical wind velocity in span of 2-4 m/s. Moreover, tip-mass rarely changes the power production while the large tip mass causes to decrease the power peaks. The suitable position for the attachment of secondary-beam is near from primary beam's unfixed end. The optimum position for the secondary beam obtained from this study is 0.75D away from the primary beam's unfixed end.

Future Enhancements

Although two parameters are studied in this research for performance analysis, change in load resistance can be studied in order to identify the effect on the performance. The experimental study can be performed by following this research for the validation of the results.

Acknowledgments

First, the authors are thankful to Units Engineering Consultancy Pvt. Ltd. as they provide the necessary platform and computational resource for carrying out the research. Also, the authors would like to acknowledge the department of Mechanical and Aerospace Engineering, Pulchowk Campus, Nepal for the cooperation, coordination and constant support to complete this research.

References

- [1] Kai Yang, Tian Qiu, Junlei Wang, and Lihua Tang. Magnet-induced monostable nonlinearity for improving the VIV-galloping-coupled wind energy harvesting using combined cross-sectioned bluff body. *Smart Materials and Structures*, 29(7):07LT01, may 2020.
- [2] Guobiao Hu, Junlei Wang, Hongwei Qiao, Liya Zhao, Zhaoyu Li, and Lihua Tang. An experimental study of a two-degree-of-freedom galloping energy harvester. *International Journal of Energy Research*, 45(2):3365–3374, feb 2021.
- [3] Che Xu and Liya Zhao. A 2DOF galloping oscillator with internal resonance for broadband concurrent wind and base vibration energy harvesting. In *Proc.SPIE*, volume 11588, mar 2021.
- [4] Marina G. López-Arias, Felix Nieto, and Santiago Hernández. Experimental study for wind energy harvesting based on the aeroelastic excitation of a semi-circular cylinder. *WIT Transactions on Engineering Sciences*, 128:139–149, 2020.
- [5] Amin Bibo and Mohammed F Daqaq. An analytical framework for the design and comparative analysis of galloping energy harvesters under quasi-steady aerodynamics. *Smart Materials and Structures*, 24(9):94006, 2015.
- [6] Chunbo Lan, Lihua Tang, Guobiao Hu, and Weiyang Qin. Dynamics and performance of a two degree-of-freedom galloping-based piezoelectric energy harvester. *Smart Materials and Structures*, 28(4):45018, 2019.
- [7] Hassan Elahi, Marco Eugeni, and Paolo Gaudenzi. A Review on Mechanisms for Piezoelectric-Based Energy Harvesters. *Energies*, 11(7), 2018.
- [8] Alper Erturk and Daniel J. Inman. *Introduction to Piezoelectric Energy Harvesting*, chapter 1, pages 1–18. John Wiley & Sons, 2011.
- [9] J P Den Hartog. *Mechanical vibrations*, 1985.
- [10] A Barrero-Gil, G Alonso, and A Sanz-Andres. Energy harvesting from transverse galloping. *Journal of Sound and Vibration*, 329(14):2873–2883, 2010.
- [11] Jayant Sirohi and Rohan Mahadik. Harvesting Wind Energy Using a Galloping Piezoelectric Beam. *Journal of Vibration and Acoustics*, 134(1), 2011.
- [12] A Abdelkefi, M R Hajj, and A H Nayfeh. Piezoelectric energy harvesting from transverse galloping of bluff bodies. *Smart Materials and Structures*, 22(1):15014, dec 2012.
- [13] Sandip Thakur, Kamal Darlami, and Laxman Poudel. Aeroelastic Energy Harvesting: A Case for Galloping. In *Proceedings of IOE Graduate Conference*, volume 8, pages 137 – 143. Institute of Engineering, Tribhuvan University, Nepal, June 2020.
- [14] Ansys fluent theory guide. Technical report, Ansys Inc., 2013.
- [15] Friedrich-Karl Benra, Hans Josef Dohmen, Ji Pei, Sebastian Schuster, and Bo Wan. A Comparison of One-Way and Two-Way Coupling Methods for Numerical Analysis of Fluid-Structure Interactions. *Journal of Applied Mathematics*, 2011:853560, 2011.
- [16] Christopher J Freitas. The issue of numerical uncertainty. *Applied Mathematical Modelling*, 26(2):237–248, 2002.